Electronic Supplementary Material (ESI) for RSC Advances.

Supporting Information

Corrosion Resistance for Superwetting Immiscible Oil/Water Separation Porous Materials

Wanting Rong[a], Haifeng Zhang[a,b,c,*], JiaMu Cao[a], Yanjing Tuo[b], Weiping Chen[a.,c], Xiaowei Liu[a,b,c]

[a] MEMS Center, Harbin Institute of Technology, Harbin 150001, China
[b] State Key Laboratory of Urban Water Resource & Environment (Harbin Institute of Technology), Harbin 150001, China
[c] Key Laboratory of Micro-Systems and Micro-Structures Manufacturing, Ministry of Education, Harbin, 150001, China
[*]Email: zhanghf@hit.edu.cn.

1.Supporting Instruments and Characterization

The X-ray photoelectron spectroscopy (XPS) measurement was carried out on a Thermo Fisher ESCALAB 250Xi photoelectron spectrometer equipped with an Al-anode at a total power dissipation of 150 W (15 kV, 10 mA), and the binding energies were referenced to the C1s line at 284.8 eV from adventitious carbon. The sample was functionally characterized by Fourier transform infrared (FT-IR) spectroscopy using a Thermo Fisher Nicolet 6700 with the KBr pellet method at room temperature in the range of 4000−400 cm^{-1}. The Raman measurements were acquired by using a Lab RAM (Aramis) system with an Ar-ion laser of 532 nm wavelength and 50 mW power. The solutions with different pH values were adjusted by adding ammonium hydroxide. The pH values were measured using a pH meter (Mettler-Toledo, Switzerland). The optical images and movies were obtained by a highspeed video camera (Sony, HDR-CX450).

2.Supporting Figures

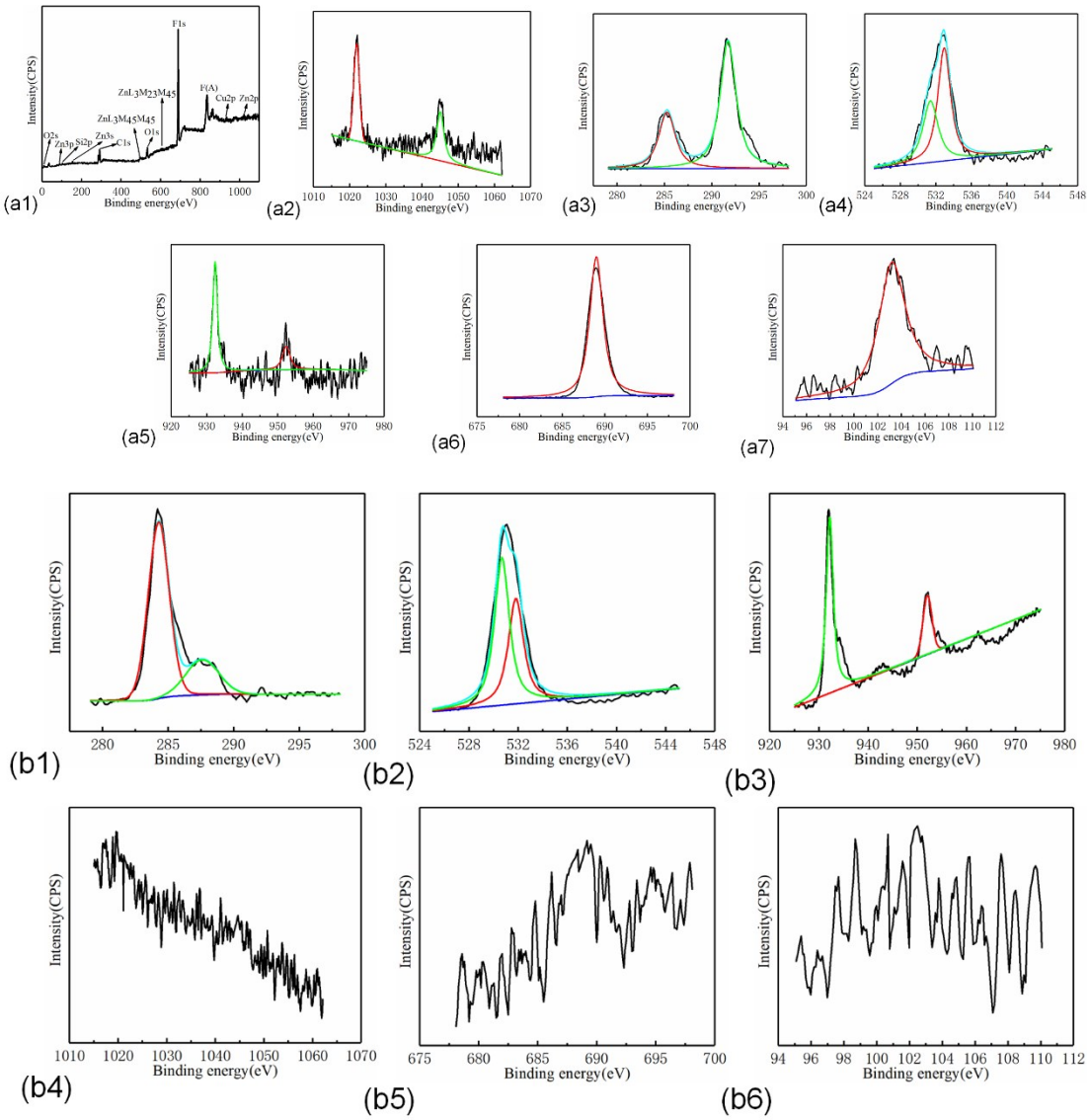

Fig. S1. (a) XPS results of the 3D porous FZCF sample. (a1) survey spectra, (a2-a7) the higher resolution curves of Zn2p spectrum, C1s spectrum, O1s spectrum, Cu2p spectrum, F1s spectrum and Si2p spectrum. (b) XPS results of the treated copper foam. (b1-b6) the higher resolution curves of C1s spectrum, O1s spectrum, Cu2p spectrum, Zn spectrum, F spectrum and Si spectrum.

The representative XPS survey spectra of the FZCF sample is shown in Fig. S1(a1). The survey spectra demonstrates the existence of Zn, C, O, Cu, F and Si elements over the sample (Fig S1(a2-a7)). The asymmetric peaks line shape shows the Zn 2p3/2 peak of the FZCF sample locates at the binding energy (BE) of 1021.20 eV and the Zn 2p1/2 peak locates at 1044.6 eV (Fig S1(a2)). Because the Zn 2p peak of metallic Zn generally locates at 1021.40 eV and 1045.1 eV [1], it can be deduced that Zn element in the FZCF exists in oxidized state, and it is in accordance with the XRD result. Furthermore, the C-H bonds at 285 eV and C-F bonds at 291.6 eV can be identified from the C1s spectrum (Fig S1(a3)). Two components with the BEs of

531.6 eV and 533.3 eV can be observed from the O1s spectrum (Fig S1(a4)). They correspond to the O atoms in ZnO matrix and C-O bond [2]. The C-F bonds at 688.7 eV and the Si-O bonds at 103 eV can be identified from the F1s spectrum and the Si2p spectrum (Fig S1(a6-a7)) [3,4]. For the copper foam substrate, typical Cu2p1/2 located at 952 eV and Cu2p3/2 located at 932.47 eV can be observed that have significantly split spin–orbit components (Fig S1(a5)) [5]. They correspond to the Cu atoms in Cu bond. The copper foam exhibits salient satellite peaks which come from copper. These results indicate that the FAS chemically bonds with the ZnO layer during the preparation and modification processes over the FZCF sample. As a comparison, the untreated copper foam sample contains three elements of C, O, and Cu without Zn, F and Si elements in Fig S1b.

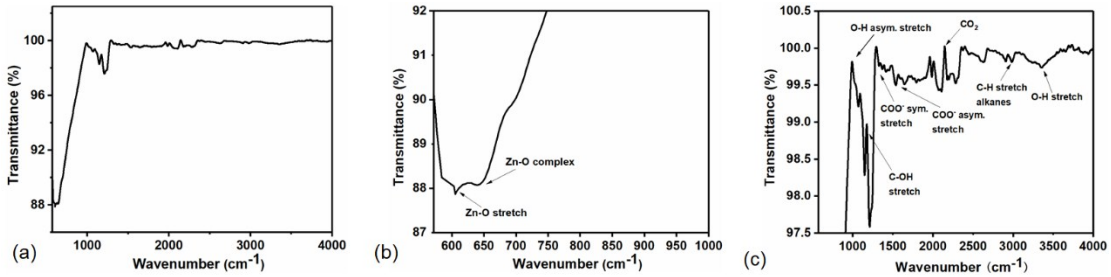

Fig S2. (a) The whole FTIR spectra of the as-synthesized FZCF sample. (b) The regional FTIR spectra of the as-synthesized FZCF sample at adsorption peaks from 550 to 1000cm^{-1}. (c) The regional FTIR spectra of the as-synthesized FZCF sample at adsorption peaks from 1000 to 4000cm^{-1}.

The FTIR spectra of the as-prepared FZCF sample is shown in Fig S2a. A series of adsorption peaks from 1000 to 4000cm^{-1} can be found corresponding to vibrations of various impurities such as hydroxyl (-OH), carboxylate (COO^-) and alkane (C-H) present on the FZCF sample surface (Fig S2c). Specifically, the most intense broad band at 3408 cm^{-1} is assigned to the O-H stretching mode of hydroxyl group in H_2O molecules. for. The presence of these bands in synthesized nanoparticles may be due to both dissociation and molecularly adsorption of atmospheric water. Peaks between 2830 and 3000 cm^{-1} are due to C-H stretching vibration of alkane groups. The peaks observed at 1630 and 1384 cm^{-1} are due to the asymmetrical and symmetrical stretching of the zinc carboxylate, respectively. The adsorption peak observed at 2300 cm^{-1} is due to the existence of CO_2 molecules in air [6]. The adsorption peak that appeared at 1200 cm^{-1} is attributed to C-OH stretching vibrations and the bands around 1034 cm^{-1} are bulges with O-H asymmetric stretching vibration modes of oxide ions in the nanocrystals [7]. The absorption bands at 576 and 468 cm^{-1} are attributed to the Zn−O stretching in the ZnO lattice in Fig S2b [8]. The carboxylate probably comes from reactive carbon containing plasma species during synthesis and the hydroxyl results from the hydrophily of the ZnO on the FZCF sample [9]. This suggests that these FTIR-identified impurities mainly exist near ZnO surfaces. The hydroxyl-terminated surfaces show comparatively higher water wetting [10,11]. The superwetting of the FZCF sample is consistent with the hydroxyl defects concentration. Due to the low hydroxyl ion concentration, the FZCF presents the outstanding superhydrophobicity to the benefit of immiscible oil/organic solvents and water separation.

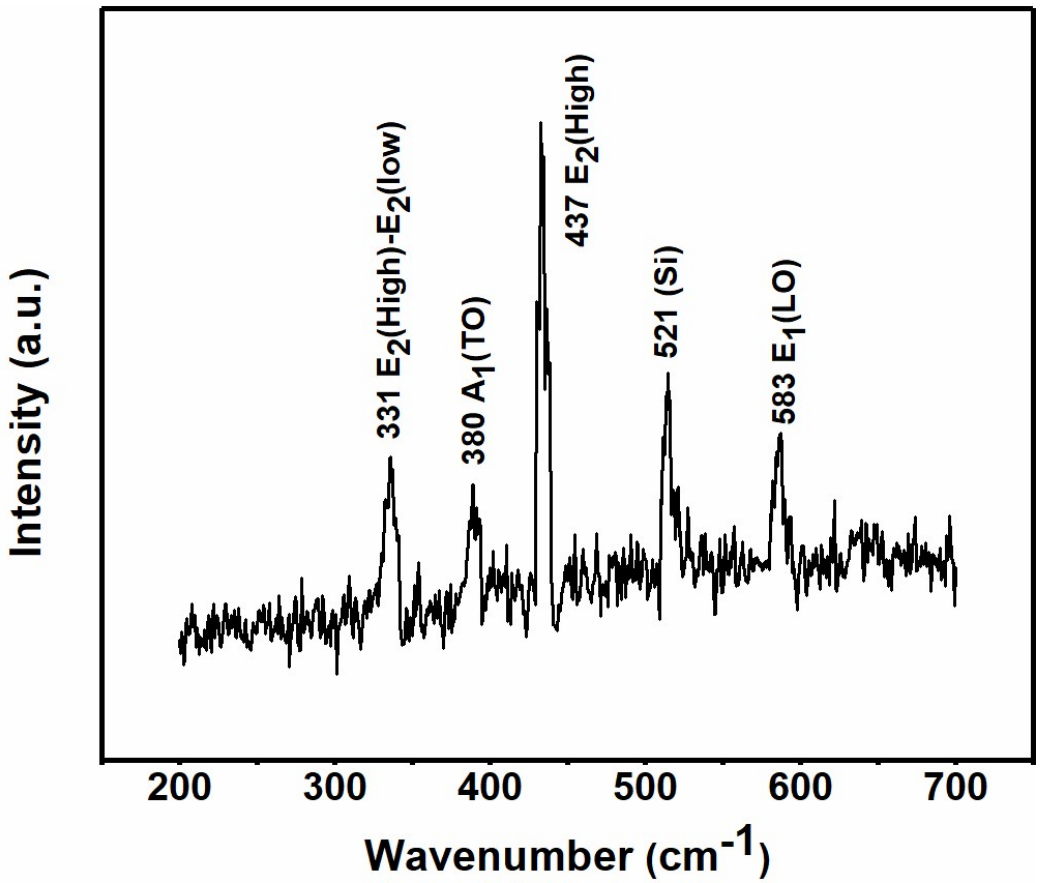

Fig S3. Raman spectra of the as-synthesized FZCF sample.

The Raman spectra of the FZCF sample is shown in Fig S3. All peaks in the Raman spectra can be demonstrated the exist of ZnO structure. The peak locates at 331 cm^{-1} is aroused by the E_2 (high)-E_2 (low) multiple scattering process of ZnO on the FZCF sample. While the band at 468 cm^{-1} of two strong absorption bands in the FTIR spectra corresponds to the E_2(high)-E_2(low) mode of hexagonal ZnO (Raman active). The main peaks at 380 cm^{-1} corresponds to A_1 (TO) and 437 cm^{-1} corresponds to the E2 (high frequency) optical phonon mode is related to oxygen atoms present in ZnO of the FZCF [12]. The high intensity of 583 cm^{-1} peak of the E_1 (LO) mode indicates its oxygen deficient nature of the ZnO in the FZCF sample, reflecting the superhydrophobicity of FZCF [13-14].

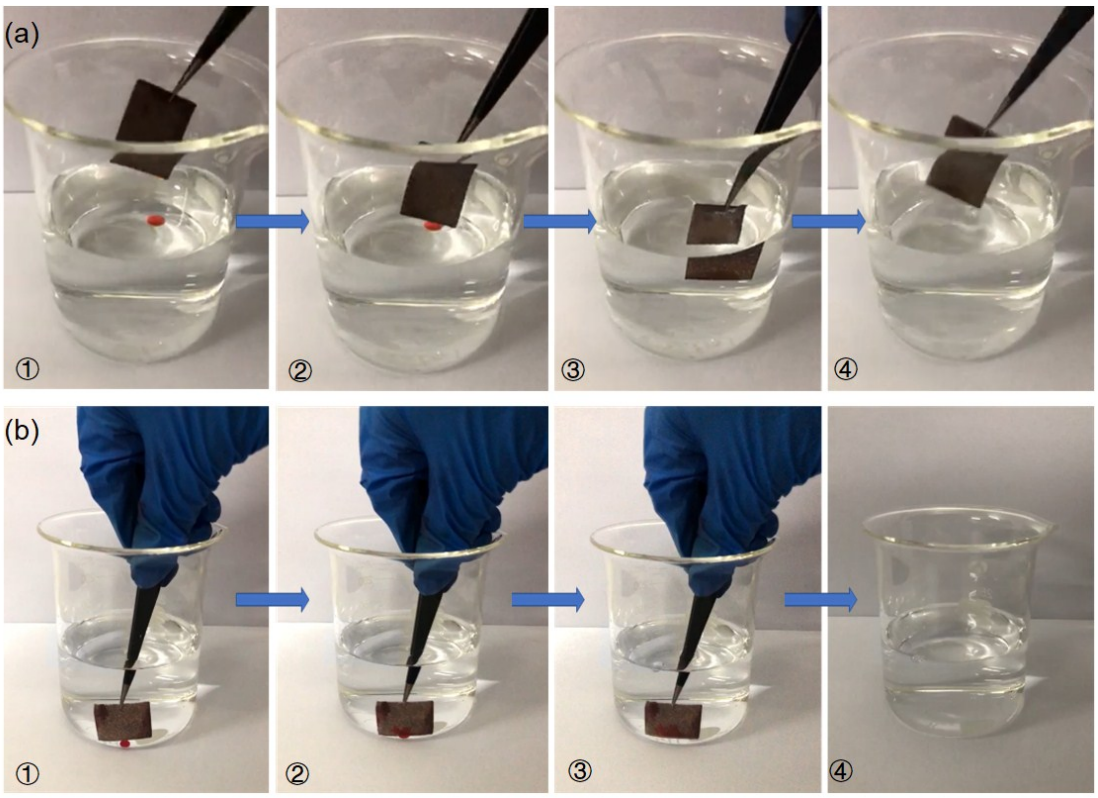

Fig. S4. Adsorption of light and heavy oils/organic solvents on water surface and underwater using the porous FZCF samples. (a) Removal of toluene (light organic solvent) on water surface by a FZCF sample: (①) toluene (dyed with Sudan III) on the as-prepared FZCF sample (brown red color), (②) the sample was immersed in water, contacted with droplets, (③) the adsorption was completed within 1 s after a the sample was dropped in, (④) the sample was taken out of the water and no residue was on the water surface. (b) Adsorption of chloroform (heavy organic solvent) under water: (① and ②) the FZCF was immersed in water to contact with chloroform (dyed with Sudan III), showing a mirror surface due to the trapped air, (③) chloroform was rapidly adsorbed when contacted with the FZCF sample, and the air inside the porous foam was driven out, (④) no residual chloroform could be observed after clean-up.

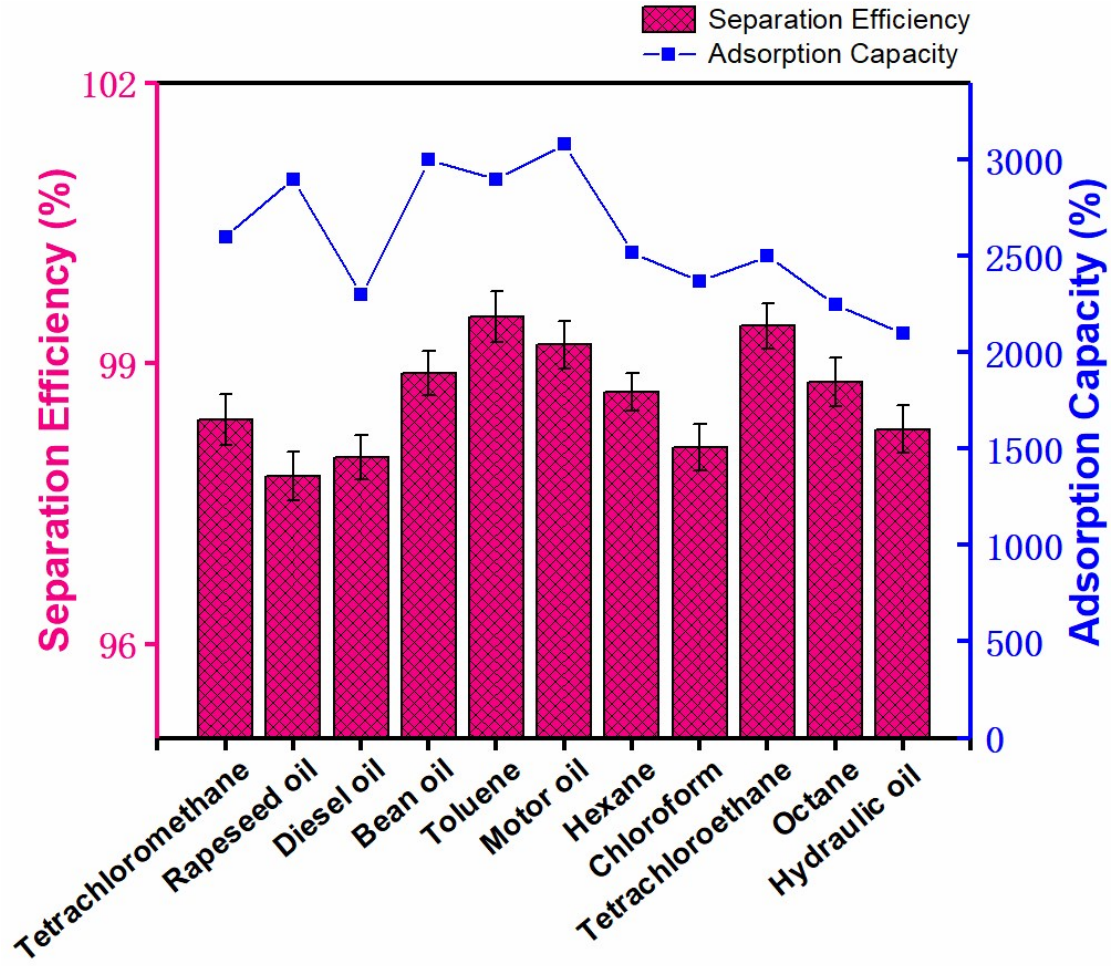

Fig. S5. The separation efficiency and adsorption capacity of porous FZCF for various oil/organic solvents.

3.Supporting Movies

Movie S1: shows eleven examples of light/heavy oils and organic solvents rapid removal from water surface and underwater velocities.
Movie S2: separation of the FZCF for immiscible oils/organic solvents and water.

References

[1] Chen, M., Wang, X., Yu, Y. H., Pei, Z. L., Bai, X. D., Sun, C., et al. X-ray photoelectron spectroscopy and auger electron spectroscopy studies of Al-doped ZnO films. *Appl. Surf. Sci.* 158 (2000) 134-140.

[2] Sun Y, Seo JH, Takacs CJ, Seifter J, Heeger AJ. Inverted polymer solar cells integrated with a low-temperature-annealed sol-gel-derived ZnO Film as an electron transport layer. *Adv. Mater.* 23 (2011) 1679-1683.

[3] Li, L., Zhang, Y., Lei, J., He, J., Lv, R., Li, N., et al. A facile approach to fabricate superhydrophobic Zn surface and its effect on corrosion resistance. *Corros. Sci.* 85 (2014) 174-182.

[4] Saleema, N., Sarkar, D. K., Gallant, D., Paynter, R. W., Chen, X. G. Chemical Nature of Superhydrophobic Aluminum Alloy Surfaces Produced via a One-Step Process Using Fluoroalkyl-Silane in a Base Medium. *ACS Appl. Mater. Interfaces*. 3 (2011) 4775-4781.

[5] Wang, Y., Lin, F., Peng, J., Dong, Y., Li, W., Huang, Y. A Robust Bilayer Nanofilm Fabricated on Copper Foam for Oil-Water Separation with Improved Performances. *J. Mater. Chem. A*. 4 (2016) 101039.

[6] Senthilkumaar, S., Rajendran, K., Banerjee, S., Chini, T. K., Sengodan, V. Influence of Mn doping on the microstructure and optical property of ZnO. *Mater. Sci. Semicond. Process.* 11 (2008) 6-12.

[7] Maensiri, S., Laokul, P., Promarak, V. Synthesis and optical properties of nanocrystalline ZnO powders by a simple method using zinc acetate dihydrate and poly (vinyl pyrrolidone). *J. Cryst. Growth*. 289 (2006) 102-106.

[8] Gandhi, V., Ganesan, R., Thaiyan, M. Effect of Cobalt Doping on Structural, Optical, and Magnetic Properties of ZnO Nanoparticles Synthesized by Coprecipitation Method. *J. Phys. Chem. A*. 118 (2014) 9715-9725.

[9] Simonsen, M. E., Li, Z., Søgaard, E. G. Influence of the oh groups on the photocatalytic activity and photoinduced hydrophilicity of microwave assisted sol-gel tio2 film. *Appl. Surf. Sci.* 255 (2009) 8054-8062.

[10] Pakdel, A., Bando, Y. Golberg, D. Plasma-Assisted Interface Engineering of Boron Nitride Nanostructure Films. *ACS Nano*. 8 (2014) 10631–10639.

[11] Xiong, G., Pal, U., Serrano, J. G., Ucer, K. B., Williams, R. T. Photoluminesence and FTIR study of ZnO nanoparticles: the impurity and defect perspective. *Phys. Status Solidi.* 3 (2010) 3577-3581.

[12] Umar, A., Kim, S. H., Lee, Y. S., Nahm, K. S., Hahn, Y. B. Catalyst-free large-quantity synthesis of ZnO nanorods by a vapor–solid growth mechanism: Structural and optical properties. *J. Cryst. Growth*. 282 (2005) 131-136.

[13] Wang, X., Li, Q., Liu, Z., Zhang, J., Liu, Z., Wang, R. Low-temperature growth and properties of ZnO nanowires. *Appl. Phys. Lett.* 84 (2004) 4941-4943.

[14] Yadav K, Mehta BR, Bhattacharya S, Singh JP. A fast and effective approach for reversible wetting-dewetting transitions on ZnO nanowires. *Sci. Rep.* 6 (2016) 35073.